International Journal of Thin Films Science and Technology

http://dx.doi.org/10.18576/ijtfst/150102

Optimization of the electrical conductivity of SnO_2 by Taguchi design and sol-gel Route for perovskite solar cells

K. J. A. Yao[1,2,3,], B. Hartiti[1], F. K. Konan[1,2,3,4], Y. Doubi[1], A. Ziti[1], A. Batan[1,5], H. Labrim[1,6], A. Laazizi[7], B. Aka[3], P. thevenin[8]*

[1] Laboratoire de Mathématiques et Sciences Physiques Appliquées aux Sciences de l'Ingénieur (MSPASI), FSTM, Université Hassan II de Casablanca (UH2C), BP 146 Mohammedia 20650, Morocco
[2] Laboratoire des Sciences Physiques Fondamentales et Appliquées, Equipe de recherche Matériaux : Energies Renouvelables et Environnement, Ecole Normale Supérieure (ENS) Abidjan, 08 BP 10 Abidjan 08, Côte d'Ivoire
[3] Laboratoire d'Energie Solaire et de Nanotechnologie (LESN) - IREN (Institut de Recherches sur les Energies Nouvelles), Université Nangui Abrogoua, 02 BP 801 Abidjan 02, Côte d'Ivoire
[4] Unité Mixte de Recherche en Science et Technique de l'Ingénieur, LIEESE (Laboratoire d'Ingénierie Électronique, d'Électricité et des Systèmes Embarqués), INP-HB, BP 1093 Yamoussoukro, Côte d'Ivoire
[5] IMERN Laboratory, SME2D Team, FST Errachidia, University Moulay Ismail of Meknes, BP 509 Boutalamine, 52000 Errachidia, Morocco
[6] Advanced Systems Engineering Laboratory, National School of Applied Sciences, Ibn Tofaîl University, B.P. 242 Kénitra, Morocco
[7] Laboratoire Modélisation et Ingénierie Multiphysique– LMIMPEquipe de recherche: Caractérisation des Systèmes et Contrôles- CSCENSAM, University Moulay Ismail, Marjane 2, B.P. 15290, Meknès, Morocco
[8] LMOPS Laboratory, University of Lorraine, Centrale Supelec - 2, rue E. Belin, B.P. 57070 Metz, France

Received: 12 Jul. 2025, Revised: 22 Sep. 2025, Accepted: 7 Nov. 2025
Published online: 1 Jan. 2026

Abstract: This work aims to optimize the electrical conductivity of SnO_2 thin films elaborated by sol-gel spin-coating coupled to Taguchi approach for electron transport in perovskite solar cells (PSC). An L9 (3^3) orthogonal array with three factors: sol-gel solution concentration in Sn^{4+}, spin-coating speed, and annealing temperature, each at three levels was used to design the experiments. Characterizations including structural (XRD), vibrational mode (Raman), surface (SEM/EDX), optical (UV-Vis), and electrical (two-point probe) analyses, as well as statistical evaluations (signal-to-noise (S/N) ratio and ANOVA), were conducted to identify an optimal synthesis condition ($A_3B_1C_3$) for the SnO_2 thin film. This combination Sn^{4+} concentration of 0.46 M, spin speed of 2500 rpm, and annealing temperature of 400°C for 2 hours represents a reproducible and economically viable protocol, yielding an electrical conductivity of $\sigma = 9.005 \times 10^{-2}$ S·cm^{-1}. Moreover, the optimized SnO_2 layer exhibits a compact rutile cassiterite structure with a homogeneous surface, an optical transparency of approximately 85.074% in the visible spectrum and a direct bandgap Eg = 3.642 eV. This combination of properties fulfills the essential criteria for efficient electron transport material (ETM) in flexible, low-cost, and temperature-sensitive PSC architectures.

Keywords: SnO_2, Taguchi L9 (3^3), ETM, electrical conductivity, ANOVA.

1. Introduction

Perovskite solar cells (PSCs), while promising among third-generation photovoltaic technologies, remain commercially constrained due to their limited long-term stability [1,2]. This instability is primarily attributed to environmental degradation (induced by humidity, oxygen, and UV exposure) and interfacial defects that hinder charge carrier mobility [3,4]. Optimizing charge transport properties particularly electron transport within the electron transport material (ETM) represents a key strategy for enhancing both the stability and performance of PSCs [5]. An ideal ETM should: i) possess high optical transparency, ii) have a conduction band well-aligned with that of the perovskite, iii) present a compact and homogeneous surface to minimize non-radiative recombination at the ETM/perovskite interface, iv) offer excellent thermal and chemical stability, v) be compatible with low-cost, moderate-temperature fabrication methods, and vi) exhibit high electrical conductivity for rapid electron extraction from the perovskite layer to the collecting electrode [6-8].

In the literature, titanium dioxide (TiO_2) is commonly used as an ETM; however, tin dioxide (SnO_2) has recently gained increasing attention as a competitive alternative to TiO_2, which remains the most widely employed material in PSC architectures [8,9]. Compared to TiO_2, SnO_2 offers the best optoelectronic properties [5,9], with a lower temperatures processing, rendering it suitable for flexible and heat-sensitive substrates [10,11]. SnO_2 thin films can elaborated via various deposition techniques and

*Corresponding author E-mail: yaokonanjeanarmand@gmail.com

preparation conditions. These techniques include sputtering [12], spray pyrolysis [13], chemical bath deposition [14], thermal evaporation [15], and the sol-gel method [16]. The latter is particularly attractive due to its simplicity, precise stoichiometric control, and compatibility with low-temperature processing. Combined with spin-coating deposition, the sol-gel method involves several interacting parameters that must be rigorously controlled [16,17]. Consequently, synthesis conditions must be meticulously managed to minimize structural defects, excessive porosity, or poor crystallinity, which could compromise the optical and electrical performance of the SnO_2 thin film [17,18]. To optimizing these interdependent properties through controlled synthesis, several prior studies have investigated the isolated effects of precursor concentration, annealing temperature, post-annealing treatments, annealing duration, on SnO_2 properties [13,19,20]. Although insightful, these approaches often overlook the simultaneous impact of factors and factor levels on the targeted property of the elaborated sample. To overcome such limitations, we employ the Taguchi method, which enables efficient exploration of multiple factors simultaneously using orthogonal experimental designs, thereby reducing the total number of required experiments compared to a full factorial design. This approach facilitates the identification of optimal parameter combinations for targeted responses. Indeed, several studies have successfully applied this method to optimize the properties (absorbance, surface morphology, electrophoretic deposition (EDP) effect, crystallite size) of thin films using various orthogonal arrays adapted to different numbers of factors and levels [21-23]. To our knowledge, few studies report the optimization of the electrical properties of SnO_2 using the Taguchi method.

In this context, the present study aims to maximize the electrical conductivity of SnO_2 thin films synthesized via sol-gel method combined with spin-coating, based on a Taguchi experimental design.

Initially, nine SnO_2 thin films were fabricated based on a Taguchi L9 (3^3) experimental design involving three synthesis parameters studied at three levels (Sn^{4+} precursor concentration, spin-coating speed, and annealing temperature), thereby reducing the number of experiments compared to a full factorial design. Secondly, the electrical conductivity of these films, evaluated after phase identification by Raman spectroscopy, was used as the response variable for a statistical analysis combining signal-to-noise (S/N) ratio and ANOVA, in order to determine the optimal deposition conditions and assess the influence of each parameter. Finally, a SnO_2 thin film was synthesized under the optimized conditions, and its structural, morphological, and particularly electrical properties were analyzed to validate the relevance of the Taguchi approach, within a reproducible, low-temperature, and cost-effective process.

2. Materials and methods

2.1. Materials

The reagents used for the chemical synthesis of SnO_2 nanoparticles are: the tin precursor $SnCl_2$, $2H_2O$, acetic acid (CH_3COOH) as a pH adjuster, ethanol (C_2H_5OH) as the solvent, and distilled water. Unlike most similar studies, which generally use $SnCl_4$ and HCl, this study favors $SnCl_2$ and CH_3COOH [15].

2.2. Taguchi orthogonal array

The orthogonal array (OA) L9 (3^3) employed for experimental design corresponds to three factors, each evaluated at three levels. Table 1 presents the investigated factors along with their respective levels. Table 2 presents rather the possible experimental combinations generated using JMP Pro version 17.0 software according to the Taguchi methodology.

Table 1: Factors and their levels for SnO_2 preparation conditions.

Symbol	Factors	Levels		
		Level 1 (-)	Level 2 (0)	Level 3 (+)
A	concentration of Sn^{4+} : $[Sn^{4+}]$	0,26 M	0,36 M	0,46 M
B	spin-coating speed : rpm	2500	3000	3500
C	annealing temperature : $T_{annealing}$	300°C	350°C	400°C

Table 2: Experimental combinations based on the Taguchi L9 (3^3) design.

Experiences	A	B	C	Configuration	Samples codes
1	0,26	2500	300	----	HYSn1
2	0,26	3000	350	-00	HYSn2
3	0,26	3500	400	-++	HYSn3
4	0,36	2500	350	0-0	HYSn4
5	0,36	3000	400	00+	HYSn5
6	0,36	3500	300	0+-	HYSn6
7	0,46	2500	400	+-+	HYSn7

8	0,46	3000	300	+0-	HYSn8
9	0,46	3500	350	++0	HYSn9

2.3. Sample preparation and characterization

The experiments were conducted under the conditions summarized in Table 2. The sol-gel solutions were prepared over two hours at 55 ± 2 °C. An initial solution consisting of $SnCl_2 \cdot 2H_2O$ dissolved in ethanol at a molar ratio of 1:18, was obtained after 15 minutes of reflux stirring. Distilled water was then slowly added (H_2O:Ac-act = 1:0.63), forming solution S1 after a few minutes of gentle stirring. The pH of each sol-gel solution was stabilized at 2.42 ± 0.10 by adding glacial acetic acid. The films were deposited onto pre-cleaned ordinary glass substrates by spin-coating for 30 sec (acceleration: 700 rpm/s), with 1 to 4 coating cycles, each followed by a pre-heating step. The thermal treatment included a pre-baking stage at 120 ± 2 °C for 15 ± 1 min and an annealing step for 120 min. Each experimental condition was duplicated. The resulting thin films were characterized by Raman spectroscopy (100-900 cm^{-1}, λ = 532 nm) and their electrical properties were measured using the two-point probe method. Figure 1 provides a schematic overview of the synthesis and characterization process based on the Taguchi design.

2.4. Statistical analysis

The selected optimization criterion was the signal-to-noise (S/N) ratio, using the "larger-the-better" approach, defined by equation (1) [22]:

$$\left(\frac{S}{N}\right)_j = -10\log\left(\frac{1}{n}\sum_{r=1}^{n}\frac{1}{Y_{rj}^2}\right) \quad (1)$$

Where: r is the experiment number, n is the number of measurements for experiment r, and $Y_{(rj)}$ is the j-th measured value in experiment r.

2.5. Validation test

Based on the statistical analysis results (S/N ratio and ANOVA) obtained from the Taguchi methodology, the optimal combination of synthesis parameters for SnO_2 thin film fabrication was identified. To validate the Taguchi model and further optimize electrical conductivity, an additional series of characterizations was performed on the optimized SnO_2 thin film beyond the initial set of measurements. This included X-ray diffraction (XRD) analysis using Cu Kα radiation (λ = 0.15406 nm), scanning electron microscopy (SEM) coupled to energy-dispersive X-ray , and UV-visible spectroscopy in the range of 300 to 900 nm. Figure 1 below provides a schematic illustration summarizing the sample synthesis and characterization process.

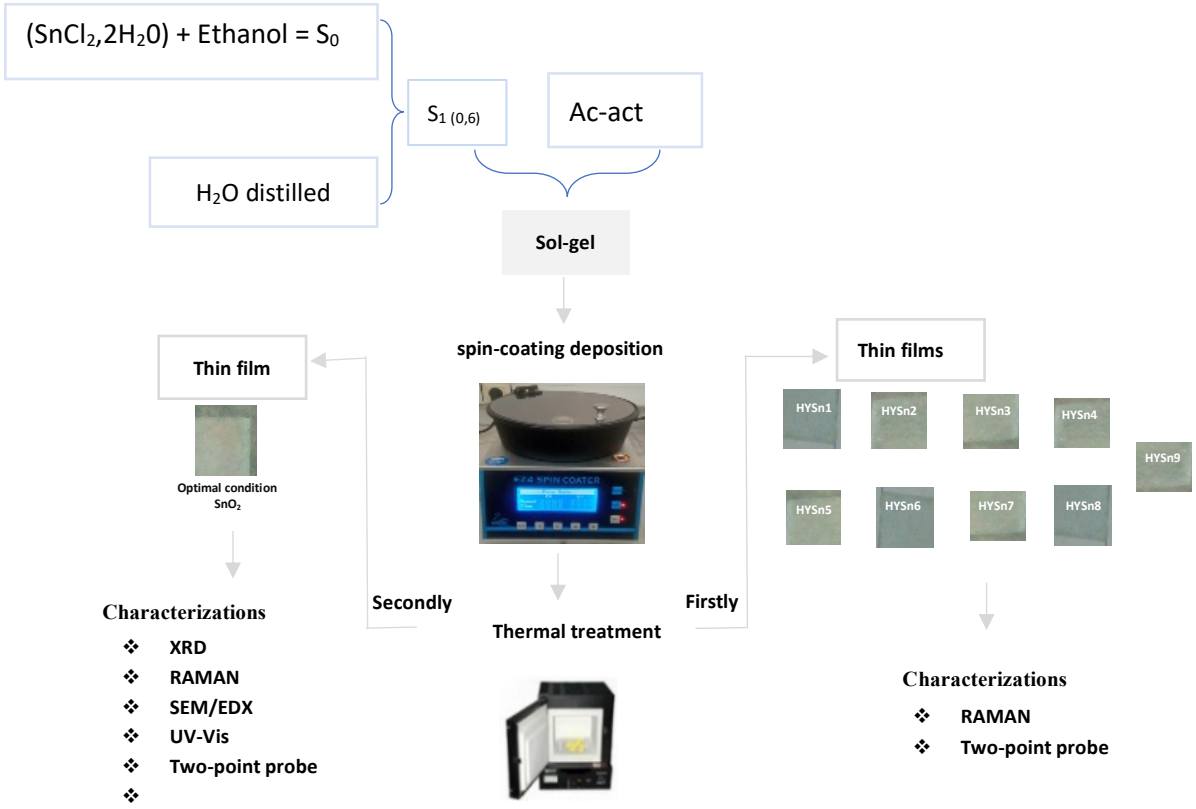

Fig. 1: Schematic illustration the sample synthesis and characterization process.

3. Results and discussion

3.1. Raman results

Figure 2 presents the Raman spectra of the nine (9) samples (HYSn1 to HYSn9) from the Taguchi table. The Raman analysis reveals the presence of the characteristic vibrational mode of rutile SnO_2 (the localized Sn-O vibration around 632 cm^{-1} with variable intensity) [24] in the majority of the synthesized SnO_2 semiconductors. Moreover, according to the synthesis conditions defined by the Taguchi L9 design, depending on the levels of factors used, for certain samples, the position of the main peak deviates from the reference value of 632 cm^{-1}. The Raman peak shifts from 632 cm^{-1} are attributed to internal strain and defect states (oxygen vacancies, cation substitutions), which distort the Sn-O bonding and alter lattice vibration frequencies [24].

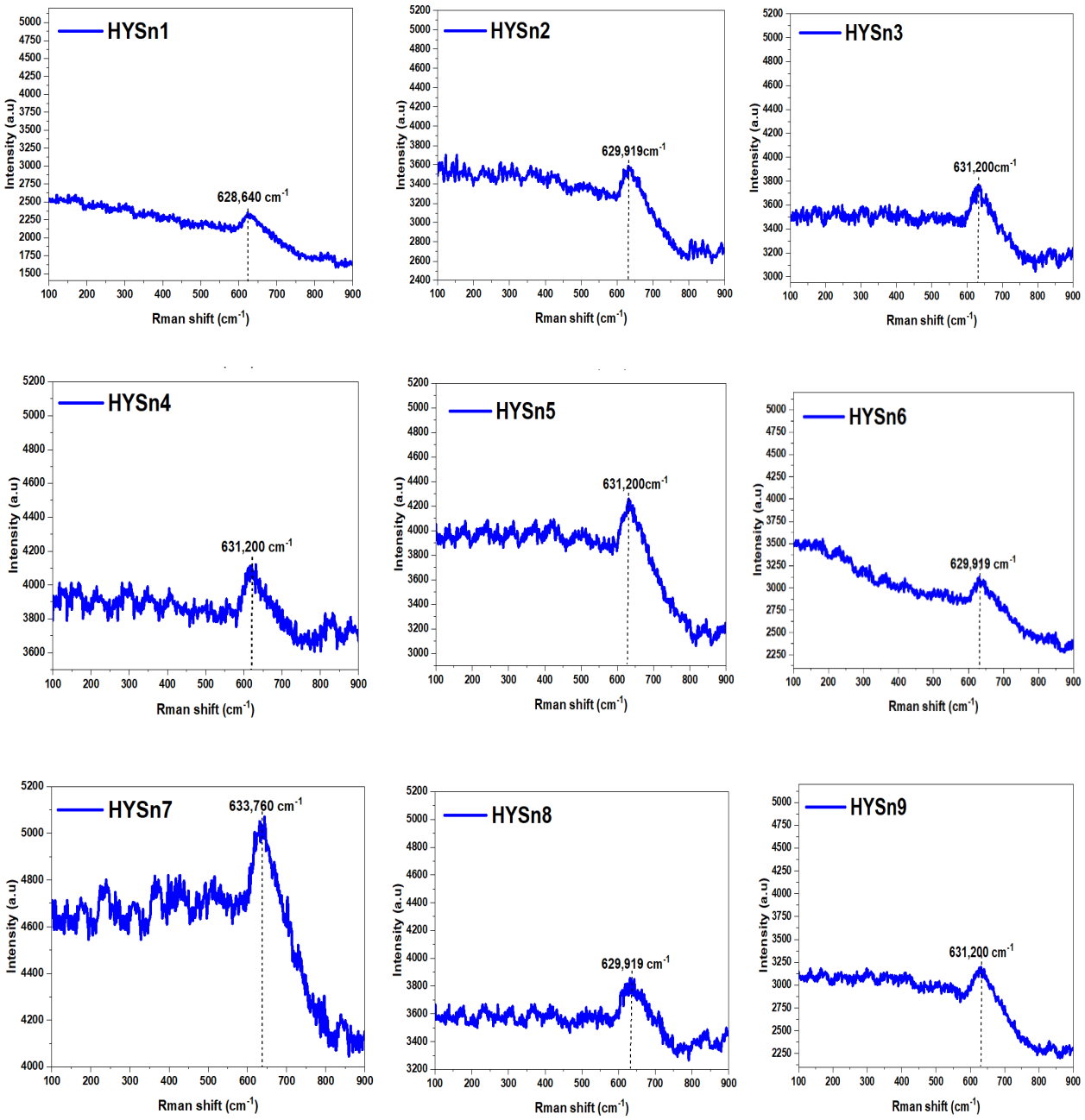

Fig. 2: Raman spectra of SnO_2 thin films for the nine samples (HYSn1 to HYSn9)

3.2. Electrical conductivity of the samples

Electrical resistivity is a fundamental physical property characterizing a material's ability to oppose the flow of electric current. This parameter is essential for electron collection and transport in perovskite solar cells [9]. It is defined as the product of the sheet resistance and the film

thickness, as expressed in equation (2) [17]:

$$\rho = R_{sheet} \times e \quad (2)$$

The electrical conductivity, which quantifies the material's ability to conduct electric current, is inversely related to resistivity and is defined as follows equation (3) [16]:

$$\sigma = 1/\rho \quad (3)$$

Based on the measured sheet resistance, directly obtained via the two-point probe technique, the values of and for each of the nine samples, and for both test repetitions, were calculated using equations (2) and (3). The results are presented in Table 3.

Where: "r"(r = 1, 2) and "j"(1 to 9) respectively denote the number of experimental measurements and the corresponding experimental line.

Table 3: Parameters R_{rj} , ρ_{rj} and σ_{rj} for the nine samples (HYSn1 to HYSn9)

Experiences	Values of $R_{sheet\ rj}$; ρ_{rj} *and* σ_{rj}					
	$R_{sheet\ 1j}$ (KΩ)	ρ_{1j} Ω. cm	σ_{1j} 10^{-2} S. cm^{-1}	$R_{sheet\ 2j}$ (KΩ)	ρ_{1j} Ω. cm	σ_{2j} 10^{-2} S. cm^{-1}
1	823,45	16,05739999	6,22765828	816,27	15,917400002	6,28243306
2	884,30	15,91740000	6,28243306	850,96	15,317399994	6,52852312
3	976,08	15,61740001	6,40311447	971,08	15,537399993	6,43608326
4	759,85	14,05739999	7,11369101	770,67	14,257400006	7,01390155
5	842,20	14,31740001	6,98450836	850,43	14,4574	6,91687302
6	1066,92	16,53740001	6,04689975	1084,99	16,817400014	5,94622236
7	718,81	13,65739999	7,32203787	714,60	13,577400006	7,36518037
8	850,13	14,87739806	6,72160458	837,56	14,65700006	6,82249239
9	953,78	15,73740000	6,35428978	962,266	15,877400001	6,29826042

The values of electrical conductivity obtained for the two tests range from 5.946.10^{-2} S.cm^{-1} to 7.365. 10^{-2} S.cm^{-1}, depending on the experimental combinations.

3.3. Statistical analysis of Taguchi parameters

3.3.1. Signal-to-Noise (S/N) ratio analysis

The variance or standard deviation SD_j of the measured responses for a given test "i" and based on "r" repetitions is determined using equation (4) [21]:

$$SD_j = \sqrt{\sum_{r=1}^{n} \frac{(y_{r,j} - \overline{y_j})^2}{r-1}} \quad (4)$$

Where: $\overline{y_j}$ represents the mean of the measured values and y_{ij} denotes an individual measured value.

Table 4 summarizes the parameters: y_{rj} corresponding at the response to be optimized (i.e., the electrical conductivity σ_{rj}); $\overline{y_j}$ the mean response of the electrical conductivity for the two trials; the standard deviation β_j; and the signal-to-noise ratio $(\frac{S}{N})_j$, for each of the nine samples. The values $\overline{y_j}$, SD_j and $(\frac{S}{N})_j$ are directly gives by software JMP pro version 17.0 after formular insertion.

Table 4: Determination of parameters y_{rj} ; $\overline{y_j}$; SD_j and $\left(\frac{S}{N}\right)_j$

Experiences	σ_{rj}		$\overline{y_j}$	Ecart type SD_j	Ratio $\left(\frac{S}{N}\right)_j$
	y_{1j}	y_{2j}			
1	6,22765828	6,28243306	6,2550456685	0,0335425	15,924359923
2	6,28243306	6,52852312	6,4054780895	0,1506987	16,126223079
3	6,40311448	6,43608326	6,419598866	0,0201891	16,150071925
4	7,11369101	7,01390155	7,0637962815	0,0611083	16,980113273
5	6,98450836	6,91687302	6,95069069	0,0414180	16,840250834
6	6,04689975	5,94622237	5,9965610595	0,0616520	15,557127062
7	7,32203787	7,36518037	7,3436091215	0,0264192	17,318078634

8	6,72160458	6,82249239	6,772048487	0,0617809	16,613678264
9	6,35428978	6,29826042	6,3262751005	0,0343108	16,022705974

3.3.2. Determination of optimum factor levels

Based on the results of the S/N ratio, the effects of each factor were analyzed and graphically represented to determine the optimal levels. Table 5 summarizes the effect of the various factors on the electrical conductivity of SnO_2, as obtained via the software JMP Pro version 17.0.

Table 5: Calculation of factor effects on electrical conductivity.

Factors	Levels			Effects of Factors
	1	2	3	$\Delta_{Max-Min}$
A	16,0669	16,4592	16,6515	0,5846
B	16,7409	16,5267	15,9100	0,8309
C	16,0317	16,3763	16,7695	0,7378

The graph illustrating the mean S/N ratio as a function of the different factors is shown in Figure 3.

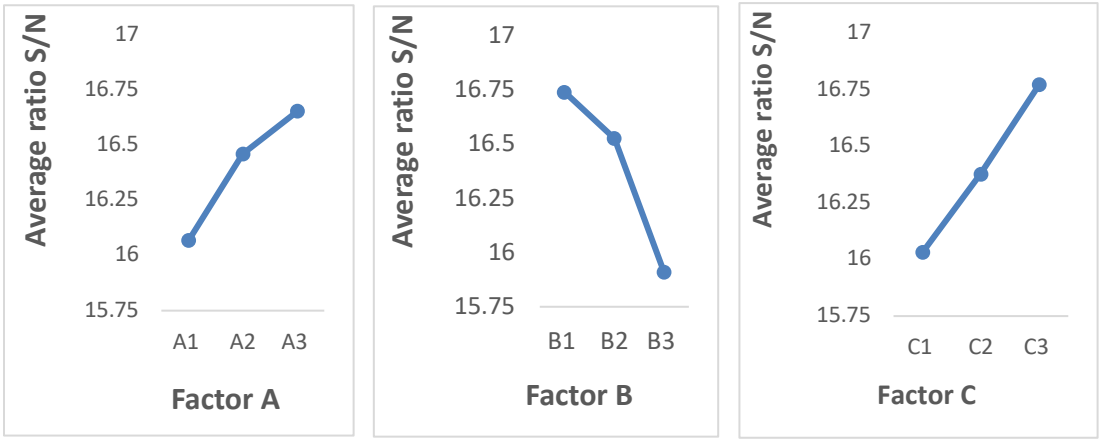

Fig. 3: Graph illustrating the mean S/N ratio as a function of the different factors

3.3.3. Determination of the optimal condition

Based on the S/N ratio effect plots (figure 3), the optimal combination of factors was determined. It is located within the experimental domain $A_3B_1C_3$, as presented in Table 6 below.

Table 6: Optimal factor levels and synthesis condition.

Controlled Factors	Optimum levels	Optimal conbinaison
A	A_3 : 0,26M	$A_3B_1C_3$
B	B_1 : 2500 rpm	
C	C_3 : 400°C	

This deposition configuration represents the most robust setup in terms of mitigating variability due to environmental disturbances or experimental error. At 2500 rpm, an optimal compromise is reached: the film is sufficiently thin to promote transparency while being dense enough to ensure efficient conductivity, as reported in previous studies [16,17]. An annealing temperature of 400°C for 2 hours activates electron conduction mechanisms by reducing trap states and enhances adhesion to the substrate [25,26]. A temperature too low would lead to an amorphous, poorly conductive film, whereas a higher temperature could cause mechanical stress or degradation [20]. A too-low concentration results in a discontinuous film, while a relatively high concentration improves layer density [13]. Other researchers have obtained different optimal combinations depending on the experimental approach and desired properties [23,25]. Thus, estimating the effect of each parameter on the response is essential. We now employ analysis of variance (ANOVA) for this purpose.

3.3.4. Analysis of variance (ANOVA)

Table 7 presents the results of the ANOVA calculations: sums of squares, degrees of freedom (ddl), variances, F-ratios, and contributions of each factor obtained directly using by JMP Pro version 17.0 software.

Table 7: ANOVA, sums of squares and contributions of each factor.

Factors	Sums of squares	ddl	Variance	F-Ratio	Contribution (%)
A	0,5326314	2	0,2663157	3,1704	21,591933
B	1,1165978	2	0,5582989	6,6463	45,2648958
C	0,8175782	2	0,4087891	4,8664	33,1431712
Error	-	-	-	-	-
Total	2,4668074	8	-	-	100

The ANOVA and contribution analysis show that spin speed is the most influential factor, followed by annealing temperature, and then Sn^{4+} ion concentration. The graph in figure 4 illustrates the contribution of each factor.

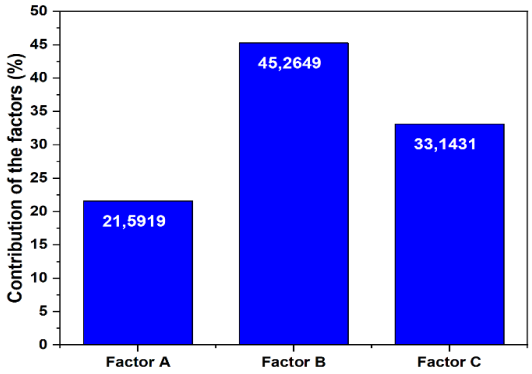

Fig. 4: Contribution of each factor

A small disparity in contributions is observed among the factors, indicating a high degree of interdependence. This means that optimization is not driven by a single factor, but by the joint adjustment of all three. The film thickness, controlled by rpm, directly impacts microstructure and compactness. The crystallinity is enhanced by annealing [20]; and the layer density is regulated by the precursor concentration [13]. This confirms the effectiveness of the Taguchi method, which maximizes performance using a limited number of experimental runs while accounting for cross-interactions.

3.4. Validation of the Taguchi test

3.4.1. Structural properties

Figure 5a shows the X-ray diffraction (XRD) patterns, and Figure 5b presents the Raman spectrum of the sample synthesized under optimal conditions.

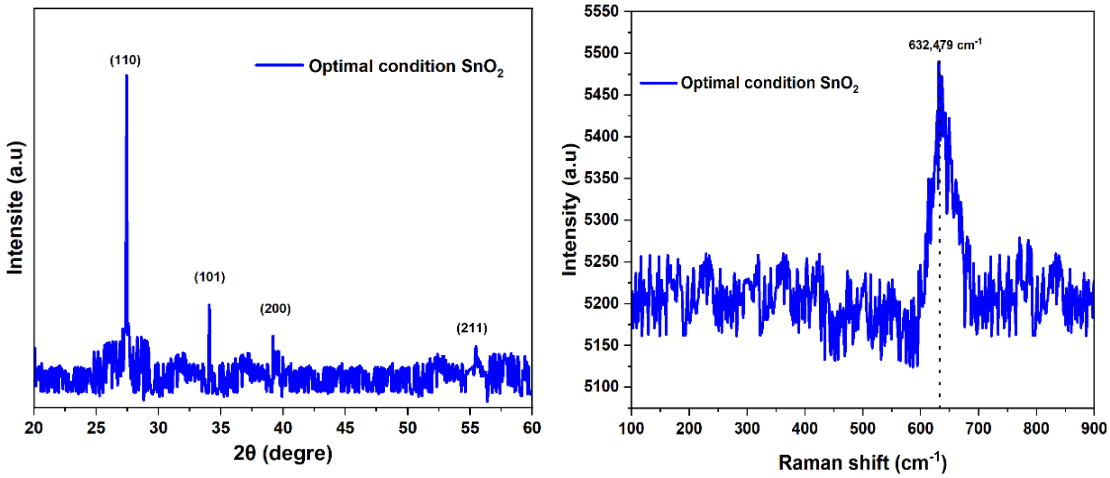

Fig. 5: a) XRD patterns and b) Raman spectrum of the SnO_2 thin film synthesized under optimal conditions.

Figure 5a displays the XRD spectrum of the SnO_2 thin film fabricated under optimal synthesis conditions, within the 2θ range of 20° to 60°. The film exhibits a polycrystalline structure, with peaks at 26.986°, 34.07°, 38.21°, and 51.40°, corresponding respectively to the (110), (101), (200), and (211) planes according to JCPDS card No. 41-1445 [14], all peaks correspond to the rutile phase of SnO_2, with no evidence of secondary phases. This confirms that the sol-gel solution was stoichiometrically stable and that crystallization at 400 °C for 2 hours was effective, supporting the purity and quality of the SnO_2 layer produced under optimal conditions.

The texture coefficient $TC(hkl)$ was calculated to quantify the degree of preferential growth along of the (110), (101), (200) and (211) planes by using Harris's method (Equation 5) [13,14].

$$TC(hkl) = \frac{\frac{I(hkl)}{I_0(hkl)}}{\frac{1}{N}\sum_{n=1}^{N}\frac{I(hkl)}{I_0(hkl)}} \quad (5)$$

$I(hkl)$ is experimental normalized intensity of the peak, $I_0(hkl)$ is relative reference intensity from the JCPDS card (card no. 41-1445) and N is number of peaks used.

The table 8 below summarizes the calculated texture coefficient $TC(hkl)$ for each peak.

Table 8: Summarizes of the calculated texture coefficient $TC(hkl)$ for each peak.

(hkl) planes	Experimental intensity (I)	JCPDS intensity (I)	I/I₀	TC(hkl)
(110)	220,64	100	1,103	2,08
(101)	51,06	57	0,440	0,83
(200)	24,88	26	0,478	0,901
(211)	20,40	100	0,102	0,19

The optimized SnO_2 film shows a preferred orientation along the (110) plane (TC(110) >1), consistent with reports from other authors [13]. This crystallographic orientation strongly influences conductivity by reducing grain boundary defects, which decreases carrier scattering and enhances mobility [17,19].

Furthermore, Figure 5b confirms the formation of a single cassiterite phase via the Raman spectrum, showing a characteristic A_1g mode at 632.479 cm^{-1} [24]. The absence of bands associated with oxygen defects or secondary phases (SnO or metallic Sn) indicates good stoichiometric control during synthesis, aligning with the XRD results and suggesting a low structural defect density favorable for electronic conduction.

3.4.2. SEM-EDX analysis

Figures 6a, 6b, and 6c respectively present the Scanning Electron Microscope (SEM) images at a scale of 5 µm (10000×) and 3 µm (20000×), as well as the Energy Dispersive X-ray (EDX) spectrum of the SnO_2 semiconductor film fabricated using the optimal combination $A_3B_1C_3$ on a glass substrate.

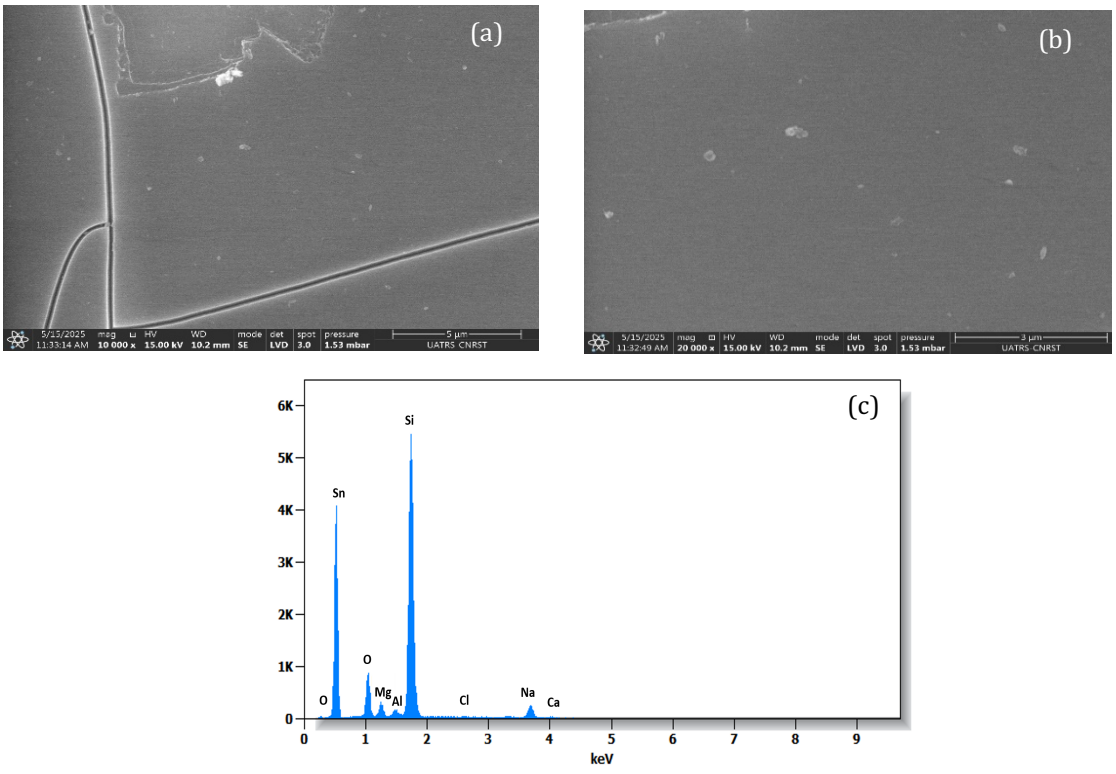

Fig. 6: a) SEM image 5µm b) SEM image 3µm c) EDX spectra of the optimal condition of the SnO_2 thin film.

The SEM images obtained for Figures 6a and 6b reveal a smooth, homogeneous surface of the optimally fabricated SnO_2 thin film. No visible porosity or significant growth defects were identified, indicating that the selected spin speed (2500 rpm) allowed for uniform spreading of the solution and well-controlled drying. This homogeneity is crucial to: i) promote efficient lateral conduction by minimizing disruptions in the transport network, ii) reduce interfacial recombination by ensuring intimate contact with the active perovskite layer, and iii) improve adhesion to the

substrate, which is essential for mechanical stability. The observed compact morphology is also favorable for reducing current leakage in solar devices, thereby enhancing the overall cell efficiency [8,27].

The table 9 below presents the chemical composition of the optimal SnO_2 thin film obtained by EDX (figure 6c).

Table 9: Elemental composition of the SnO_2 thin film

Chemical elements	C	O	Na	Mg	Sn	Al	Si	Cl	Ca	Total
Weight (%)	0,80	32,33	3,90	2,24	38,53	0,70	18,40	0,20	2,90	100
Atom (%)	0,4	42,08	9,50	3,80	23,21	0,50	17,51	0,30	2,70	100

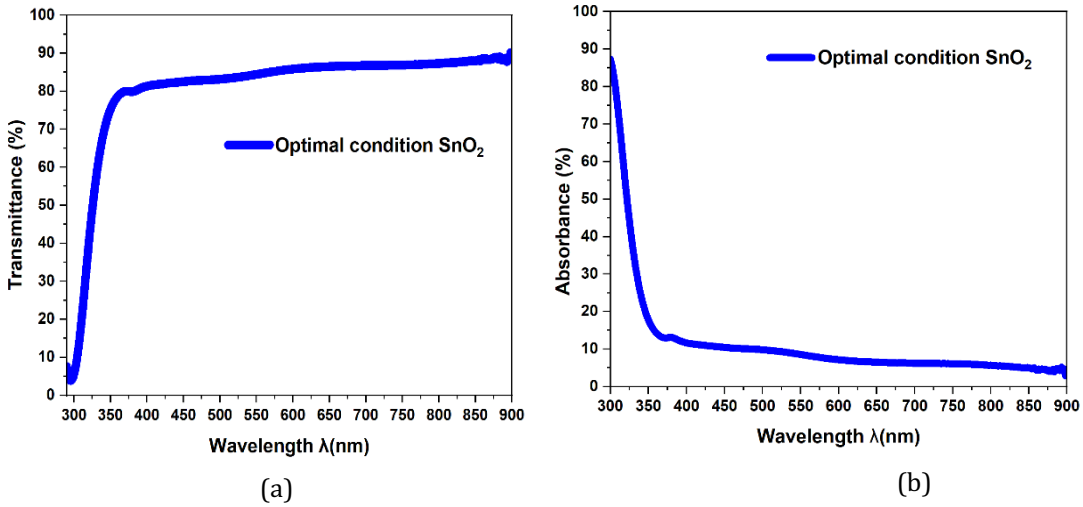

Fig. 7: Optimal SnO_2 condition: a) transmittance spectra b) absorbance spectra

The EDX analysis reveals the predominant presence of tin (Sn) and oxygen (O) elements, with the atomic proportions of tin (Sn) and oxygen (O) corresponding to an O/Sn stoichiometry close to 2, confirming the expected formation of the SnO_2 compound. The low chlorine content (<1%) suggests an almost complete elimination of the chlorinated residue from the $SnCl_2$ precursor thanks to the thermal treatment at 400°C for 2 hours. Similarly, the observed traces of carbon (< 0.5%) are likely due to atmospheric contamination or organic residues on the surface, which is common in thin films prepared by the sol-gel method. The elements: silicon (Si), sodium (Na), and calcium (Ca) detected are related to the ordinary glass substrate used. These results are consistent with the data reported in the literature [13,20].

3.4.3. Electrical properties

Table 10 presents the electrical characterization results (sheet resistance, electrical resistivity, and conductivity) of the optimized SnO_2 films, calculated based on equations (2) and (3).

Table 10: Electrical parameters for the optimal SnO_2 condition.

Optimal condition SnO_2	R_{sheet} (KΩ)	ρ (Ω. cm)	σ (x 10^{-2} S. cm^{-1})
	578,370	11,104	9,005

The results obtained for the optimal SnO_2 condition (sheet resistance, electrical resistivity, and conductivity) were found to be superior to those obtained under other conditions [13,14,17]. The low resistivity indicates efficient ohmic transport, ensuring effective electron extraction toward the cathode. The electrical conductivity of 9.005 S/cm represents a significant improvement compared to typical values for undoped SnO_2 fabricated at low temperatures [13,14]. This value is considered suitable for ETL applications, especially when compared to intrinsic TiO_2 layers fabricated under similar conditions [9,15].

3.4.4. Optical properties

Studying the optical properties of the optimized SnO_2 thin film further validates the quality of the obtained layer.

3.4.4.1. Transmittance and absorbance

The transmittance (T) and absorbance A(λ) spectra were measured using a UV-Vis spectrophotometer. Figures 7a and 7b presents respectively the transmittance and absorbance A(λ) spectra for the optimal SnO_2 condition. The transmittance of the SnO_2 layer fabricated under the optimal condition $A_3B_1C_3$ shows an average transmittance of approximately 85.408 % in the visible range (400 - 800

nm) and 62.153% in the UV range (300 - 400 nm).

These results, significantly better than those reported in certain studies [17,29], are suitable for solar cell applications where visible transmittance above 85% is recommended [12]. **3.4.4.2. Optical bandgap**

The optical absorption coefficient α(λ) was calculated using the Beer-Lambert law, as expressed in equation (6) [28]:

$$\alpha(\lambda) = 2{,}303 \times A(\lambda) / e \quad (6)$$

A(λ) is the absorbance and e is the film thickness.

The corresponding absorption coefficient is about 2.375 × 10^{-6} cm^{-1} in the UV and 6.090 × 10^{-7} cm^{-1} in the visible. The direct optical bandgap (Eg) was determined using the Tauc relation defined by equation (7) [29]:

$$(\alpha h\nu)^2 = A(h\nu - E_g) \quad (7)$$

A is a constant, hυ is the photon energy, and α is the absorption coefficient as defined in equation (6). The values of Eg were estimated from the linear extrapolation of $(\alpha h\upsilon)^2$ versus hν plots to the hν axis. Figure 8 illustrates the $(\alpha h\nu)^2$ versus hυ curve for the optimal SnO_2 condition.

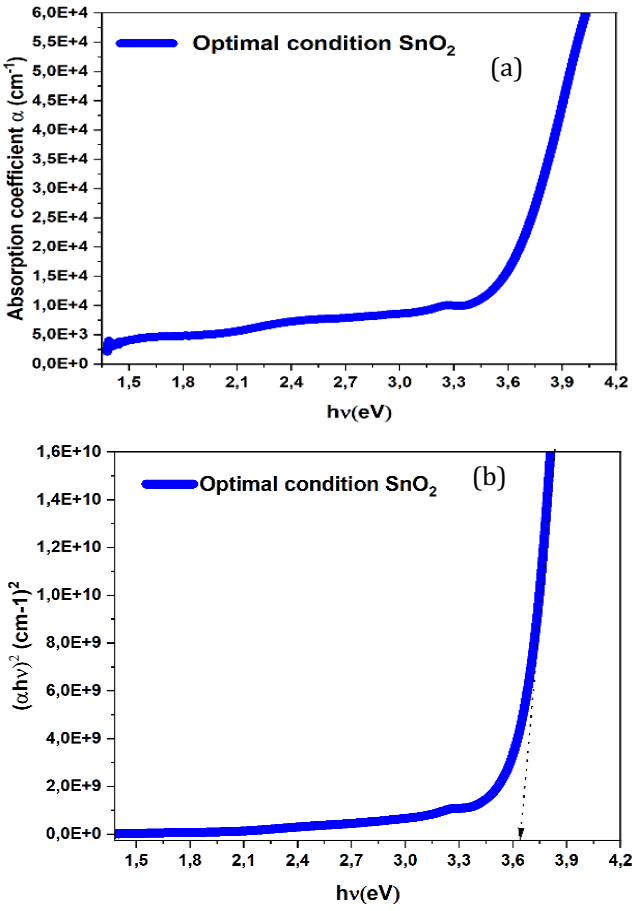

Fig. 8: Optimal condition SnO_2 : a) absorption coefficient spectra b) $(\alpha h\upsilon)^2$ versus hυ curve.

The extracted direct bandgap of 3.642 ± 0,1 eV agrees well with the reported value for rutile-phase crystalline SnO_2. This value ensures optimal alignment of the intrinsic SnO_2 ETM with the energy levels of the perovskite active layer, as reported in the literature [6,8,29] is consistent with results from other studies using more complex fabrication techniques [28].

4. Conclusion

The optimization of electrical conductivity of tin oxide (SnO_2) was successfully investigated by using a sol-gel spin-coating method combined with a Taguchi L9 (3^3) approach. The best performance was achieved with the parameter combination $A_3B_1C_3$, corresponding to a precursor concentration of 0.46 M, a spin speed of 2500 rpm, and an annealing temperature of 400°C for 2hours. This configuration led to the formation of a compact cassiterite-phase rutile SnO_2 thin film with a homogeneous surface. A significantly improved electrical conductivity of approximately 9.005 S/cm was obtained, confirming the effectiveness of the optimization strategy under cost-effective synthesis conditions. Complementary analyses revealed a high optical transparency (>85%), an optical bandgap of 3.642 eV± 0,1 eV. The SnO_2 thin film optimized demonstrate high potential to replace conventional TiO_2, offering advantages in terms of optoelectronic performance, thermal compatibility, and low-temperature fabrication for using as an electron transport material in perovskite solar cells.

Author contributions

The first draft of the manuscript was written by **K. J. A. Yao**. All authors contributed to the study conception and design, data collection, as well as the analysis and discussion of the results. These tasks were carried out by **B. Hartiti, F. K. Konan, Y. Doubi, A. Ziti, A. Batan, H. Labrim, A. Laazizi, B. Aka and P. Thevenin**

Funding

No funding was received for the completion of this study.

Data availability

The authors confirm that the data supporting the findings of this study are available from the corresponding author upon reasonable request.

Conflicts of interest statement

The authors declare that there is no conflict of interest regarding the publication of this paper.

References

[1] E. K. Solak, and E. Irmak. (2023). Advances in organic photovoltaic cells: a comprehensive review of

materials, technologies, and performance. *RSC advances* **13 (18),** 12244-12269, (2023). https://doi.org/10.1039/D3RA01454A

[2] A. Machín, and F. Márquez, (2024). Advancements in photovoltaic cell materials: silicon, organic, and perovskite solar cells. *Materials* **17 (5),** 1165, (2024) https://doi.org/10.3390/ma17051165

[3] M. K. Rao, D. Sangeetha, M. Selvakumar, Y. Sudhakar, and M. Mahesha, (2021). Review on persistent challenges of perovskite solar cells' stability. *Solar Energy* **(218),** 469-491, (2021). https://doi.org/10.1016/j.solener.2021.03.005

[4] H. Mohseni, M. Dehghanipour, N. Dehghan, F. Tamaddon, M. Ahmadi, and M. Sabet, (2021). Enhancement of the photovoltaic performance and the stability of perovskite solar cells via the modification of electron transport layers with reduced graphene oxide/ polyaniline composite. *Solar Energy* **(213)** 59-66. (2021). https://doi.org/10.1016/j.solener.2020.11.017

[5] L. Lin, T. W. Jones, T. C. Yang, N. W. Duffy, J. Li, L. Zhao, B. Chi, X. Wang, and G. J. Wilson, (2021). Inorganic electron transport materials in perovskite solar cells, *Advanced Functional Materials* **31 (5),** 2008300. (2021). https://doi.org/10.1002/adfm.202170032.

[6] S. Foo, M. Thambidurai, P. S. Kumar, R. Yuvakkumar, Y. Huang, and C. Dang, (2022). Recent review on electron transport layers in perovskite solar cells. *International Journal of Energy Research*. **46(15),** 21441- 21451 2022:1-11, (2022). https://doi.org/10. 1002/er.7958

[7] Q. Fatima, A. A. Haidry, H. Zhang, A. El Jery, and M. Aldrdery, (2024). A critical review on advancement and challenges in using TiO2 as electron transport layer for perovskite solar cell. *Materials Today Sustainability*, 100857, (2024) https://doi.org/10.1016/j.mtsust.2024.100857

[8] A. Uddin, and H. Yi, (2022). Progress and Challenges of SnO2 Electron Transport Layer for Perovskite Solar Cells: A Critical Review. *Solar RRL* 6 (6), 2100983, (2022) https://doi.org/10.1002/solr.202100983

[9] Y. Liao, Y. Chang, T. Lin, K. Lee and M. Wu, (2024). Recent Advances in Metal Oxide Electron Transport Layers for Enhancing the Performance of Perovskite Solar Cells. *Materials*, **(17),** 2722 (2024). https://doi.org/10.3390/ma17112722

[10] M. R. Kim, H. W. Choi, and C. W. Bark, (2020). Low-temperature thermally evaporated SnO2 based electron transporting layer for perovskite solar cells with annealing process. *Journal of Nanoscience and Nanotechnology* **20 (9),** 5491-5497, (2020). https://doi.org/10.1166/jnn.2020.17620

[11] J. Bahadur, A. H. Ghahremani, B. Martin, S. Pishgar, T. Druffel, M. K Sunkara, and K. Pal, (2019). A study on the material characteristics of low temperature cured SnO2 films for perovskite solar cells under high humidity. *Journal of Materials Science: Materials in Electronics* **(30),** 18452-18461, (2019) https://doi.org/10.1007/s10854-019-02199-8

[12] C. R. Onyeagba, M. Islam, P. K. Yarlagadda, T. Tesfamichael, (2023). Investigating the properties of tin-oxide thin film developed by sputtering process for perovskite solar cells. *Materials for Renewable and Sustainable Energy* **12 (1),** 31-37, (2023) https://doi.org/10.1007/s40243-022-00226-z

[13] A. Abdelkrim, S. Rahmane, O. Abdelouahab, N. Abdelmalek, and G. Brahim, "Effect of solution concentration on the structural, optical and electrical properties of SnO2 thin films prepared by spray pyrolysis. *Optik* **127 (5),** 2653-2658, https://doi.org/10.1016/.jleo.2015.11.232 (2016).

[14] N. Suwannakham, A. Tubtimtae, and E. Wongrat, (2023). Structural, linear/non-linear optical, optoelectrical, and electrical properties of novel crystalline antimony-doped tin oxide thin films synthesized by the chemical deposition. *Physica B: Condensed Matter* **(649),** 414440, (2023) https://doi.org/10.1016/j.physb.2022.414440

[15] W. Bin, W. Huang, W. Lin, and H. Lee, (2021). Study on optical and electrical properties of thermally evaporated tin oxide thin films for perovskite solar cells. *Crystals* 11 (11), 1380, (2021). https://doi.org/10.3390/cryst11111 380

[16] S. Soumya, R. Vinodkumar, and N. Unnikrishnan. (2021). Conductivity type inversion and optical properties of aluminium doped SnO2 thin films prepared by sol-gel spin coating technique. *Journal of Sol-Gel Science and Technology* **99 (3)**, 636-649 (2021) https://doi.org/10.1007/s10971-021-05599-7

[17] P. Sivakumar, H. S. Akkera, T. R. K. Reddy, Y. Bitla, V. Ganesh, P. M. Kumar, G. S. Reddy, and M. Poloju (2021). Effect of Ti doping on structural, optical and electrical properties of SnO2 transparent conducting thin films deposited by sol-gel spin coating. *Optical Materials* **(113),** 110845. (2021) https://doi.org/10.1016/j.optmat.2021.110845

[18] M. A. Dheyab, A. A. Aziz, M. S. Jameel, and N. Oladzadabbasabadi (2022). Recent advances in synthesis, modification, and potential application of tin oxide nanoparticles. *Surfaces and Interfaces* **(28),** 101677, (2022). https://doi.org/10.1016/j.surfin.2021.101677

[19] J. L. Alves do Nascimento, L. Chantelle, I. M. Garcia dos Santos, A. L. Menezes de Oliveira, and M. C. F.

Alves. (2022). The Influence of Synthesis Methods and Experimental Conditions on the Photocatalytic Properties of SnO2: A Review," *Catalysts* **12 (4),** 428, (2022). https://doi.org/10.3390/catal12040428

[20] S. Hakeem, S. Ali, M. A. Liaqat, A. Jamshed, M. Basit, M. T. Masood, and S. Javed. (2024). Effect of Annealing Temperature on the Morphology, Structure and Optical Properties of Spin-Coated SnO2 Films for Solar Cell Application. *Materials Proceedings* **17 (1),** 28 (2024) https://doi.org/10.3390/materproc2024017028

[21] Y. Liu, and T. Zeng (2023). Evaluation of the effects of synthesis conditions on the crystallite size of SnO2 nanoparticles via the Taguchi method. *Inorganic Chemistry Communications* **(156),** 111257 (2023) https://doi.org/10.1016/j.inoche.2023.111257

[22] W. Chen, M. C. Uribe, E. E. Kwon, K. A. Lin, Y. Park, L. Ding, L. H. Saw (2022). A comprehensive review of thermoelectric generation optimization by statistical approach: Taguchi method, analysis of variance (ANOVA), and response surface methodology (RSM). *Renewable and Sustainable Energy Reviews* **(169),** 112917 (2022) https://doi.org/10.1016/j.rser.2022.112917

[23] Y. Doubi, B. Hartiti, M. Siadat, H. Labrim, S. Fadili, M. Stitou, M. Tahri, A. Belfhaili, P. Thevenin, and E. Losson. (2022). Optimization with Taguchi Approach to Prepare Pure TiO2 Thin Films for Future Gas Sensor Application. *Journal of Electronic materials* **51 (7),** 3671-3683 (2022) https://doi.org/10.1007/s11664-022-09615-6

[24] B. Eifert, M. Becker, C. T. Reindl, M. Giar, L. Zheng, A. Polity, Y. He, C. Heiliger, and P. J. Klar. (2017). Raman studies of the intermediate tin-oxide phase. *Physical Review Materials* **1(1),** 014602, (2017) https://doi.org/10.1103/PhysRevMaterials.1.014602

[25] G. Joshi, J. K. Rajput, and L. Purohit. (2020). Improved stability of gas sensor by inclusion of Sb in nanostructured SnO2 thin films grown on sodalime. *Journal of Alloys and Compounds* **(830)**, 154659, (2020).https://doi.org/10.1016/j.jallcom.2020.154659

[26] H. Chenaina, C. Messaadi, J. Jalali, and H. Ezzaouia (2021). Study of structural, optical and electrical properties of SnO2 doped TiO2 thin films prepared by a facile Sol-Gel route. *Inorganic Chemistry Communications*, **(124),** 108401, (2021) https://doi.org/10.1016/j.inoche.2020.108401

[27] H Tao, Z Ma, G Yang, H Wang, H Long, H Zhao, P Qin, G Fang. (2018) Room-temperature processed tin oxide thin film as effective hole blocking layer for planar perovskite solar cells. *Applied Surface Science,* **(434),** 1336-1343 (2018) https://doi.org/10.1016/j.apsusc.2017.11.161

[28] GG Riungu, SW Mugo, JM Ngaruiya, GM John, N Mugambi (2021) Optical Band Energy, Urbach Energy and Associated Band Tails of Nano Crystalline TiO2 Films at Different Annealing Rates. *American Journal of Nanosciences*; **7(1),** 28-34 (2021) https://doi.org/10.11648/j.ajn.20210701.15

[29] P Sivakumar, HS Akkera, TRK Reddy, GS Reddy, N Kambhala, NNK Reddy. (2021) Influence of Ga doping on structural, optical and electrical properties of transparent conducting SnO2 thin films. *Optik,* ***(226)***, 165859 (2021) https://doi.org/10.1016/j.ijleo.2020.165859